Line-shape studies in high-resolution stimulated resonance Raman spectroscopy and application to accurate determinations of hyperfine splittings in I_2

Ch. J. Bordé,* G. Camy, N. Courtier, F. du Burck, A. N. Goncharov, and M. Gorlicki**

Laboratorie de Physique des Lasers, Unité de Recherche Associée au Centre National de la Recherche Scientifique 282, Université Paris-Nord, Villetaneuse, France

Received July 5, 1995

We studied stimulated resonance Raman transitions between hyperfine sublevels of the ground electronic state $X^1\Sigma_{0^+g}(v = 0, J = 13)$ of I_2. Resonances narrower than 10 kHz (HWHM) were obtained. A detailed theoretical and experimental analysis of the line shape is presented. The pressure broadening of Raman resonances was found to be 7 ± 1 kHz/mTorr. The role of the beam divergence was investigated and shown to yield only a small broadening but some asymmetry of the lines. In the transit-time limit the theory predicts that the slow molecules should play a dominant role, as in saturation spectroscopy. Our experimental conditions are very close to that regime, and we discuss the improvements that should be made in order to reach it in future experiments. Finally, six hyperfine splittings of the ground state of I_2 were determined with a 0.2-kHz accuracy.

1. INTRODUCTION

Stimulated resonance Raman (SRR) processes have been widely used for high-precision spectroscopy of atoms and molecules,[1] especially when the levels of interest are metastable. Because of the long lifetime of these levels, one can obtain extremely narrow SRR resonances, which are of great interest both for spectroscopic and metrological applications.[2] When the metastable levels are hyperfine sublevels of the same ground electronic state with a frequency interval of a few hundred megahertz, it is possible to use only one laser and an acousto-optic modulator (AOM) to obtain two laser beams with proper frequencies and to avoid the laser frequency jitter problem. Thanks to this simplification, it should be much easier to obtain subkilohertz SRR resonances. There is a close analogy between the SRR interaction of a three-level system with two laser beams at frequencies ν_1, ν_2 and the interaction of the two ground-level hyperfine states with a microwave radiation at the frequency $\nu_1-\nu_2$. Owing to this analogy, our experiment has some common features with optical-microwave double resonance,[3] but it provides a better signal-to-noise ratio and uses a simpler experimental setup. This analogy becomes rigorous when the concept of effective Hamiltonian may be used.[1] This is the case when either the detuning from the intermediate level or the relaxation constant of this level is much larger than its other evolution frequencies. In this case the intermediate level can be eliminated adiabatically. In our case the Doppler shift associated with the intermediate level is usually larger than the two previous quantities, and there is no equivalent two-level system. Furthermore, the Doppler broadening, which is small but finite for the microwave transition, can be completely eliminated for the SRR transition. Numerous theoretical papers have been written on line shapes in spectroscopy of three-level systems, taking into account only relaxation decay rates and the first-order Doppler effect.[4] Generalized expressions of the susceptibility applicable to all nonlinear processes were given in Refs. 5 and 6. In this paper we extend these previous line-shape calculations to include transit-time effects in the case of SRR spectroscopy. These calculations are based on the diagrammatic representation of the density-matrix equations described in Ref. 7 and follow closely earlier derivations of the Doppler-free two-photon line shape[8] and the saturated absorption line shape.[9] This technique provides a set of computation rules associated with a double time-ordered Feynman diagram representing a given process. It includes all effects resulting from the molecular motion and especially transit-time effects that become dominant at the highest resolution. Indeed, we find that in the transit-time broadening limit the SRR resonance has a double-exponential line shape with a sharp top. As in the case of saturated absorption, this phenomenon can be explained by a slow-velocity-selection effect.[9,10] Such a line shape was already found in the case of Doppler-free two-photon spectroscopy[8] and was also pointed out in the case of SRR spectroscopy by Thomas *et al.*,[11] taking into account only the transverse Gaussian amplitude profile of the beams at a given point along the propagation axis. As far as the divergence of the laser beam is concerned, the behavior of SRR resonances differs strongly from the case of saturated absorption. We show that the SRR resonance probes the local size of the laser beam and is relatively insensitive to the beam divergence or to wave-front distortions by cell windows. So, with a beam diameter of the order of 1 cm in a low-pressure gas cell, one could obtain

0740-3224/96/0901837-12$10.00

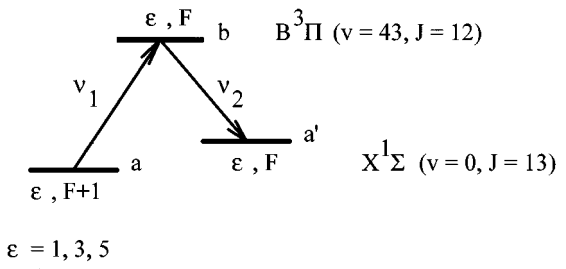

Fig. 1. Schematic representation of the SRR interaction process involving hyperfine sublevels of the X ($v = 0$, $J = 13$) state in iodine.

subkilohertz SRR resonances useful both for high-precision spectroscopy and metrology.

In this paper we illustrate this great potentiality of SRR spectroscopy by its application to the study of hyperfine structure of the ground electronic state of I_2. We observed SRR transitions between hyperfine sublevels of the ground electronic state $X^1\Sigma_{0^+g}$ ($v = 0$, $J = 13$) of this molecule. Resonances narrower than 10 kHz (HWHM) were obtained. We measured six hyperfine transitions with a 0. 2-kHz accuracy. A pressure broadening of the SRR transitions equal to 7 ± 1 kHz/mTorr was found and interpreted in terms of relevant relaxation constants. To test the small influence of the laser beams' divergence and to check our line-shape calculations, a specific experiment was made with a beam divergence angle as large as 0.5°. The results of the calculations show a remarkable quantitative agreement with the experiment.

2. EXPERIMENTAL SETUP AND RESULTS

Figure 1 shows the diagram of hyperfine sublevels in which a SRR transition is induced by two radiations at the frequencies ν_1 and ν_2. The sublevels of interest are the same as in the case of crossover resonances with a common upper level b.[12] The experimental setup is shown in Fig. 2. The laser beam at the frequency ν_2 is provided by a monomode Ar^+ laser. The beam at the frequency ν_1 is generated from the previous one by two acousto-optic modulators. In order to reduce the beams' misalignment introduced by the frequency modulation and by the frequency scanning of ν_1, we use the acousto-optic modulator AOM2 in a double-pass geometry. The acousto-optic modulator AOM1 provides the optical isolation of the laser from backscattering and increases the range of available detunings. The perpendicularly polarized beams at frequencies ν_1 and ν_2 are recombined in a Glan prism. To reduce the errors induced by the relative misalignment of laser beams and to decrease the transit-time broadening of resonances, we use an expansion of the laser beams up to a radius $w_0 \simeq 1$ cm. The I_2 pressure in the 50-cm-long cell is controlled by the thermostabilization of the cell cold finger. Our signals are detected by monitoring the unmodulated laser beam at the frequency ν_2, which is resonant with the weak transition ($\Delta F = 0$). To reduce the influence of technical amplitude noise of the laser, we use the usual differential detection method. First-derivative-type resonance signals are obtained by FM modulation ($f_{\mathrm{mod}} = 5$ kHz) with the AOM2 generator followed by phase-sensitive detection. For avoiding background signals coming from intensity changes associated with frequency modulation and frequency scanning, the laser beam at the frequency ν_1 is rejected by a second Glan prism. The laser frequency is locked to a strong hyperfine component ($\Delta F = \Delta J$) of I_2 close to the weak-transition frequency. Generally, this detuning is smaller than 20 MHz. In the case of the $(5, 10) \rightarrow (5, 9)$ transition (see Table 1) used for most line-shape studies, this detuning was much smaller. In this case we used a frequency-stabilization scheme with a saturation beam frequency shifted in comparison to the probe laser beam in the reference iodine cell. Using the hyperfine component a_2 for laser frequency stabilization with a 172.4-MHz blue-shifted saturation beam, we tuned

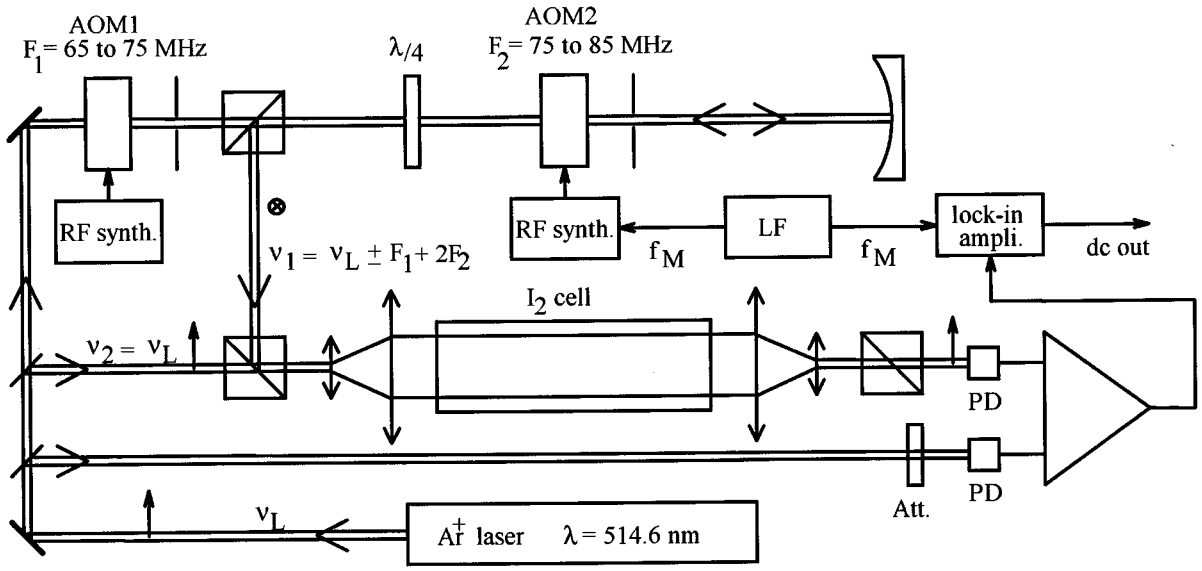

Fig. 2. Schematic representation of the experimental setup: RF, radio frequency; LF, low-frequency generator; PD's; photodiodes.

Table 1. Stimulated Resonance Raman Transitions between Hyperfine Sublevels in the X ($v = 0$, $J = 13$) State of I_2

ε', $F' \rightarrow \varepsilon''$, F''	Results of Ref. 3 (kHz)[a]	Our Result (kHz)[a]
5, 13→5, 14		75 377.5(2)
5, 11→5, 12		87 249.1(2)
5, 15→5, 14	100 892.7(4)	100 892.4(2)
3, 15→3, 14	212 479.3(4)	212 479.0(2)
5, 13→5, 12	218 699.0(4)	218 699.0(2)
5, 10→5, 9	228 679.1(1)	228 679.2(2)

[a] Numbers in parentheses are estimated reproducibilities in units of 0.1 kHz.

the laser frequency to the ($J'' = 13$, $F'' = 9$, $\varepsilon'' = 5$) → ($J' = 12$, $F' = 9$, $\varepsilon' = 5$) weak transition. Only a minor modification of our previous laser-frequency-stabilization scheme[13] was necessary in order to obtain this blue shift by means of AOM's.

Figure 3 shows a typical signal corresponding to the SRR transition between the hyperfine sublevels ($\varepsilon = 5$, $F = 10$) and ($\varepsilon = 5$, $F = 9$). The recording was made under the conditions that we usually had for the line-center measurements: The I_2 pressure was 2 mTorr; the powers of the laser beams in the cell were 4 and 8 mW at frequencies ν_1 and ν_2, respectively, with a beam-waist radius equal to 0.5 cm; the amplitude of the frequency modulation was 10 kHz.

To measure the pressure broadening of the SRR resonances, we increased the pressure of I_2 from 0.3 to 60 mTorr. The resonance shapes were fitted by Lorentzian derivatives whose widths were extrapolated to vanishing laser power and amplitude of the modulation. Figure 4 presents the resonance half-width $\gamma_{a'a}/2\pi$ versus the pressure of I_2. We found a linear dependence of $\gamma_{a'a}/2\pi$ with the iodine pressure. The slope coefficient is equal to

$$d(\gamma_{a'a}/2\pi)/dP_{I_2} = 7 \pm 1 \text{ kHz/mTorr}.$$

This result, when compared with those obtained in Ref. 14 for the population decay rate $d(\gamma_a/2\pi)/dP_{I_2} = 5 \pm 1$ kHz/mTorr (for an I_2 pressure $\geqslant 30$ mTorr), is consistent with a rather small influence of the dephasing collisions on this type of transition in iodine molecules.

The half-width of the narrowest resonance, which we obtained, is $\gamma_{a'a}/2\pi \cong 8$ kHz [Fig. 5(a)] under the following conditions: iodine pressure, 0.2 mTorr, amplitude of the modulation, 3 kHz; laser power in the cell, ~ 4 mW ($w_0 \approx 1$ cm). This value may be explained by a residual misalignment of the laser beams and, more probably, by a small uncontrolled amount of foreign gas in the cell. Under these conditions the absorption coefficient in the 50-cm-long cell corresponding to the SRR process was measured to be 0.5×10^{-6}.

We used SRR spectroscopy for the measurement of transition frequencies in the state X ($v = 0$, $J = 13$) of I_2. According to the possibilities of our AOM's, six transitions could be studied. In Table 1 we compare our results with those of Yokozeki and Muenter,[3] which were obtained in a molecular-beam double-resonance experiment. The agreement between the values is better than 1 kHz and illustrates the accuracy of our measurements. Within the accuracy of our experiment we did not find any pressure shift of the SRR resonances.

To illustrate the small influence of the beam divergence, we recorded the line shape of the SRR resonance with a beam expander out of focus. Figure 6 presents the line shapes of the SRR resonance with beam divergence angles θ equal to 0.43° (curve a), 0° (curve b), and −0.5° (curve c). The I_2 pressure in the cell was 0.3 mTorr. The solid curves (Fig. 6) are the results of line-shape calculations. The calculated line shapes, as well as the experimental ones, show an asymmetry but no significant broadening (the usual saturated absorption resonance broadening under these conditions is equal to 2.5 MHz). The small difference between the experimental and the theoretical line shapes may be explained by the frequency modulation that was used for phase-sensitive detection and by the fact that, for such a big divergence ($\theta \simeq 0.5°$), one should take into account the change of the transverse geometry of the beam along the propagation axis inside the cell.

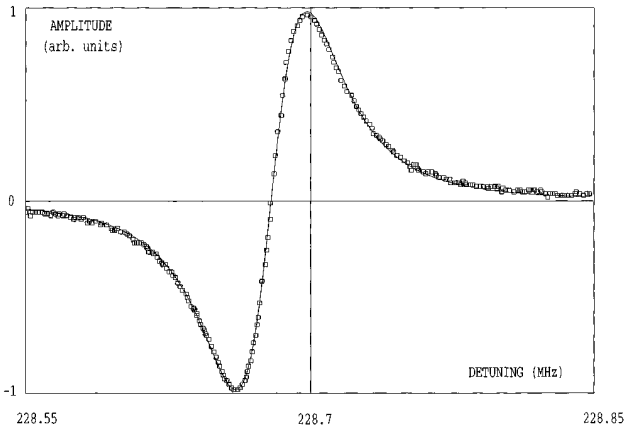

Fig. 3. SRR resonance between hyperfine sublevels ($\varepsilon = 5$, $F = 10$) and ($\varepsilon = 5$, $F = 9$). The lock-in amplifier time constant was 0.1 s. The solid curve is the first derivative of a pure Lorentzian with a half-width equal to 30 kHz.

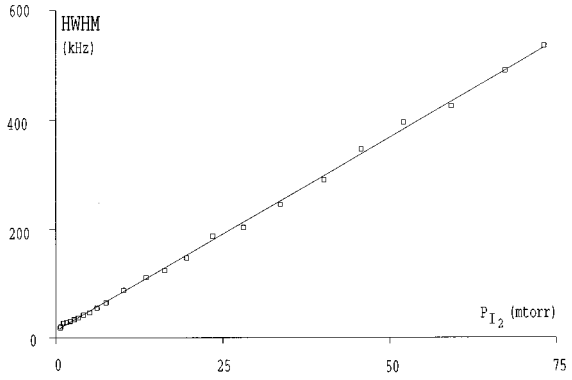

Fig. 4. Half-width of the SRR resonance fitted by a Lorentzian derivative versus iodine pressure in the cell. The solid line represents $\gamma_{a'a}/2\pi = 13.6$ kHz + 7.08 kHz/mTorr × P_{I_2} (result of a linear regression). The experimental values of the resonance half-widths at pressures greater than 35 mTorr were obtained without a telescope.

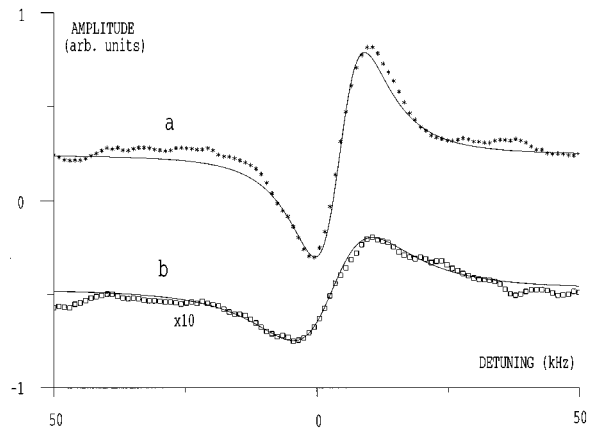

Fig. 5. Curve a, Narrowest SRR resonance recorded under the following conditions: iodine pressure $P_{I_2} \approx 0.2$ mTorr, power of the laser beams approximately 4 mW, beam diameter $2w_0 = 2$ cm, time constant equal to 3 s, and accumulation of nine 150-s sweeps. The solid curve is the first derivative of a pure Lorentzian with a half-width of ≈ 8 kHz. Curve b, Line shape of the resonance with a 0.5-cm-diameter aperture and a power density $I_{l,2} \approx 0.1$ mW/cm^2 (time constant equal to 3 s, accumulation of thirty 150-s sweeps). The solid curve is the first derivative of a pure Lorentzian with a half-width equal to 14 kHz.

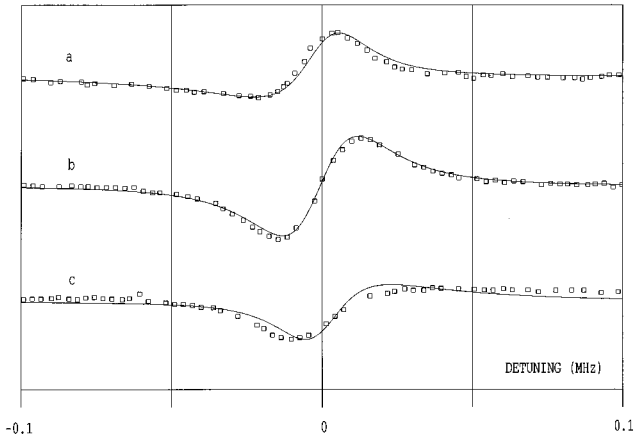

Fig. 6. Line shapes of the SRR resonances with beam divergence angles θ equal to (curve a) 0.43°, (curve b) 0, and (curve c) −0.5°; the solid curves are the results of the line-shape calculation with $\gamma_{a'a}/2\pi = 15$ kHz.

Because iodine is a very heavy molecule, it is difficult to observe transit-time effects with a laser-beam radius of the order of 1 cm. Under the conditions of the narrowest resonance [see Fig. 5(a)], a 0.5-cm-diameter aperture was installed in the 2-cm-diameter beam, and the power of the laser beam in the cell was reduced to 0.4 mW. Figure 5 (curve b) shows the first-derivative line shape of the SRR resonance thus obtained, compared with the first derivative of a pure Lorentzian with a half-width (HWHM) equal to 14 kHz (solid curve). The transit-time broadening of the SRR resonance can be observed but without any other essential change of the line shape.

3. THEORETICAL ANALYSIS: LINE-SHAPE DERIVATION FOR STIMULATED RESONANCE RAMAN SPECTROSCOPY

In this paper we limit ourselves to the three-level system that is shown in Fig. 1. It is well known (see Table 1 of Ref. 6) that, for copropagating waves under quasi-resonance conditions, the signal for such a system consists of three Doppler-free contributions: (1) a saturation signal involving the population in the intermediate level b, (2) a Raman term involving the off-diagonal matrix elements of the two lower states as the intermediate step, and (3) a dynamical Stark effect. In the present case, at the highest resolution, the first contribution gives rise to a broad, weak signal, and we discuss it only in the context of pressure broadening of our resonances at high pressure, when $\gamma_a, \gamma_{a'} \simeq \gamma_b$. Under usual experimental conditions, its size, compared with the Raman signal, is roughly in the ratio of the relaxation constants $\gamma_{aa'}/\gamma_{ba} \simeq 0.1$. In the present experiments this ratio is further squared in the case of first-derivative signals. The third term (dynamical Stark effect) is proportional to $k_1 - k_2$ and is completely negligible here.

The complete line shape is derived in the appendix with the diagrammatic representation of the density-matrix equations described in Ref. 7. As mentioned earlier, this technique provides a set of computation rules associated with a double time-ordered Feynman diagram or a density-matrix diagram representing a given process. It includes all effects resulting from the molecular motion: transit effects through the beam geometry $U(x, y, z)$ including beam curvature, first- and second-order Doppler effects, and recoil shifts ($\delta = \hbar k^2/2M$). In addition, it takes into account the relaxation mechanisms through decay rates ($\gamma_{\alpha\beta}$) and velocity-changing collisions as well as various aspects of the interaction physics, polarization and frequency modulation of the laser beam, and, at higher order, light shifts and power broadening. Finally, it is easy to introduce a general molecular phase space distribution $F(x, y, z, v_x, v_y, v_z)$.

Taking into account the saturation and Raman contributions, the final result for the absorbed power per unit length is [see Eqs. (A15), (A18), and (A34) in Appendix A]

$$dW/dz = -(n_a^{(0)}/g_a)\hbar\omega_2(2\sqrt{\pi}/ku)S(z)\Pi_\Omega I(\Delta), \tag{3.1}$$

where the various quantities are defined in Appendix A: $n_a^{(0)}$ is the lower-state equilibrium population, $S(z)$ is a geometrical factor, and Π_Ω is the product of four Rabi frequencies. When summed over Zeeman sublevels, this last product gives an angular factor analogous to that of the corresponding crossover resonance given in Ref. 12. The line shape $I(\Delta)$ is given by

$$\begin{aligned} I(\Delta) = \mathrm{Re} \int_0^{+\infty} d\tau \int_0^{+\infty} d\tau' \exp[(i\Delta - 2\gamma_{ba})\tau] \\ \times \{\exp(-\gamma_b\tau')/(1 + A_s u^2\tau'^2 + 2B_s u^2\tau\tau' \\ + C_s u^2\tau^2) + \exp[(i\Delta - \gamma_{a'a})\tau']/(1 + A_R u^2\tau'^2 \\ + 2B_R u^2\tau\tau' + C_R u^2\tau^2)\}, \end{aligned} \tag{3.2}$$

with $\Delta = (\omega_1 - \omega_2) - \omega_{a'a}$. The first term of the sum

in the integral corresponds to the saturation signal (two single-photon steps with copropagating waves), and the second term corresponds to the Raman (folded two-photon) signal. The saturation signal has exactly the same form as in the case of counterpropagating waves except for the definition of the detuning Δ. Introducing the exponential integral function E_1, the line shape may also be written as a single integral:

$$I(\Delta) = 1/(2u^2)\mathrm{Im}\Bigg(\int_0^{+\infty} \mathrm{d}\tau\{\gamma_b[\exp(Z_{S2})E_1(Z_{S2}) - \exp(Z_{S1})E_1(Z_{S1})]/(A_S Y_S) + (\gamma_{aa'} - i\Delta) \times [\exp(Z_{R2})E_1(Z_{R2}) - \exp(Z_{R1})E_1(Z_{R1})]/(A_R Y_R)\} \times \exp[(i\Delta - 2\gamma_{ba})\tau]\Bigg), \tag{3.3}$$

where

$$\begin{aligned} Z_{S1,R1} &= X_{S,R} + iY_{S,R}, \\ Z_{S2,R2} &= X_{S,R} - iY_{S,R}, \\ X_S &= \gamma_b\tau(B_S/A_S), \\ X_R &= \tau(\gamma_{aa'} - i\Delta)(B_R/A_R), \\ Y_S &= \gamma_b/(u\sqrt{A_S})\sqrt{1 + D_S u^2\tau^2}, \\ Y_R &= (\gamma_{aa'} - i\Delta)[1/(u\sqrt{A_R})]\sqrt{1 + D_R u^2\tau^2}, \\ D_{S,R} &= C_{S,R} - B_{S,R}^2/A_{S,R}. \end{aligned}$$

In Eqs. (3.2) and (3.3) the influence of the laser beams' geometry comes through the coefficients $A_{S,R}$, $B_{S,R}$, $C_{S,R}$, and $D_{S,R}$. Using Eq. (3.3), one can calculate the line shape for an arbitrary geometry of the laser beams (different positions of the waists and different values of the confocal parameters), taking into account both saturation and Raman terms. For matched beams ($w_{01} = w_{02} = w_0$, $z_{01} = z_{02} = z_0$, and $b_1 = b_2 = b$) we have $l_1 = l_2 = l$ and

$$\begin{aligned} A_S = A_R &= \frac{l + l^*}{2} = \frac{1}{w^2(z)} = A, \\ B_S = B_R &= l^* = \frac{1}{w^2(z)}\left(1 - 2i\,\frac{z - z_0}{b}\right) = B, \\ C_S = C_R &= 2l^* = C, \\ D_S = D_R &= \frac{1}{w_0^2} = D. \end{aligned} \tag{3.4}$$

In this case, the line shape (3.2) becomes

$$I(\Delta) = \mathrm{Re}\int_0^{+\infty}\mathrm{d}\tau\int_0^{+\infty}\mathrm{d}\tau'\,\exp[(i\Delta - 2\gamma_{ba})\tau] \times \frac{\exp(-\gamma_b\tau') + \exp[(i\Delta - \gamma_{a'a})\tau']}{1 + Au^2\tau'^2 + 2Bu^2\tau\tau' + Cu^2\tau^2}. \tag{3.5}$$

Close to the beam waist ($z - z_0 \ll b$),

$$1 + Au^2\tau'^2 + 2Bu^2\tau\tau' + Cu^2\tau^2 \cong 1 + \frac{\tau'^2 + 2\tau\tau' + 2\tau^2}{\tau_{\mathrm{tr}}^2}, \tag{3.6}$$

with $1/\tau_{\mathrm{tr}}^2 = (u/w_0)^2 = Au^2$.

It is also possible to derive the line shape corresponding to a misalignment between the laser beams considered as plane waves:

$$U_1(\mathbf{r}) = 1, \quad U_2(\mathbf{r}) = \exp(-k_x x). \tag{3.7}$$

A simple calculation along the lines of Appendix A gives

$$I(\Delta) = \frac{1}{2\gamma_{ba} - \gamma_{a'a}}\frac{\sqrt{\pi}}{k_x u}\,\mathrm{Re}\left[w\left(\frac{\Delta + i\gamma_{a'a}}{k_x u}\right) - w\left(\frac{\Delta + 2i\gamma_{ba}}{k_x u}\right)\right] + \frac{1}{\gamma_b}\frac{\sqrt{\pi}}{k_x u}\,\mathrm{Re}\left[w\left(\frac{\Delta + 2i\gamma_{ba}}{k_x u}\right)\right], \tag{3.8}$$

where $w(z) = \exp(-z^2)\mathrm{erfc}(-iz)$ is the error function of complex arguments. The first term corresponds to the Raman diagram and the second one to the saturation diagram. Unfortunately, no simple line shape includes both the Gaussian structure of the beams and their misalignment.

In the high-pressure limit, $\gamma_a, \gamma_{a'} \simeq \gamma_b$, and one needs to take into account both contributions in Eqs. (3.5) and (3.8). In these conditions, transit-time effects are negligible with usual laser beams ($w_0 \sim$ millimeters). If $1/\tau_{\mathrm{tr}}$, $u\sqrt{A}, u\sqrt{B}, k_x u \ll \gamma_{ba}, \gamma_b, \gamma_{a'a}$, the denominator of Eq. (3.5) is ≈ 1; the Voigt profiles in Eq. (3.8) reduce to Lorentzian shapes, and both Eqs. (3.5) and (3.8) for the line shape simplify to

$$I(\Delta) = \frac{2\gamma_{ba}}{(2\gamma_{ba})^2 + \Delta^2}\left(\frac{1}{\gamma_b} - \frac{1}{2\gamma_{ba} - \gamma_{a'a}}\right) + \frac{\gamma_{a'a}}{\gamma_{a'a}^2 + \Delta^2}\frac{1}{2\gamma_{ba} - \gamma_{a'a}}, \tag{3.9}$$

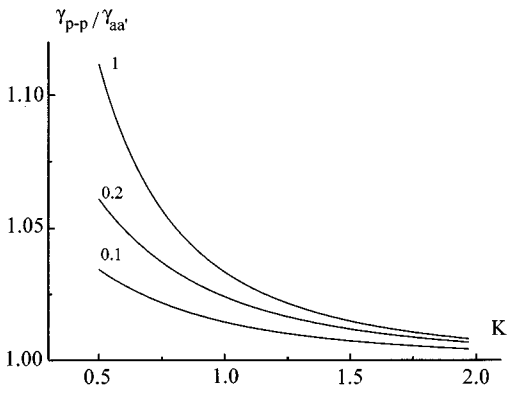

Fig. 7. Peak-to-peak width of the calculated line shape γ_{p-p} ($\gamma_{p-p} = \delta\sqrt{3}/2$, where δ is the interval between the maximum and the minimum of the derivative) versus $K = \gamma_b/\gamma_a$ for three values of the phase-mismatch parameter d defined by $\gamma_{ba} = [1 + d][\gamma_b + \gamma_a]/2$.

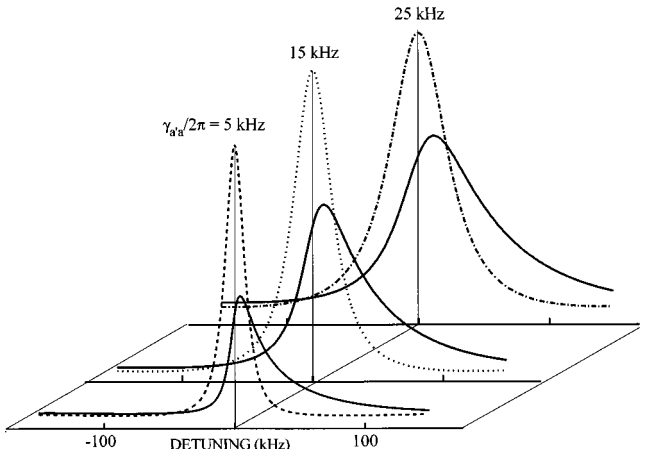

Fig. 8. Results of the line-shape calculations for SRR resonances with matched divergent beams close to our experimental conditions ($\theta = \lambda/\pi w_0 \approx 0.5°$ and $w = 0.5$ cm) compared with nondivergence cases (dashed curves) for three value of $\gamma_{a'a}/2\pi$: 5, 15, and 25 kHz.

which is the sum of two Lorentzians. When $\gamma_{a'a} \ll \gamma_{ba}$, the observed signal is a narrow Raman resonance given by $I_R(\Delta) \approx (1/2\gamma_{ba})[\gamma_{a'a}/(\gamma_{a'a}^2 + \Delta^2)]$ superimposed on the weak, broad background of the saturation signal. But we can check that, in the case where $2\gamma_{ba} = \gamma_a + \gamma_b$ and $\gamma_{a'a} = \gamma_a = \gamma_{a'}$ (no dephasing collisions), the line shape given by Eq. (3.9) becomes also a pure Lorentzian with a half-width equal to $\gamma_{a'a}$ without any condition on the ratio $\gamma_{a'a}/\gamma_{ba}$. (This corresponds to the possibility to interchange the two middle vertices in both diagrams of Appendix A.) We analyzed the peak-to-peak width of the first derivative of the line shape given by Eq. (3.9) when dephasing collisions become important. Figure 7 shows the peak-to-peak width γ_{p-p} versus the parameter $K = \gamma_b/\gamma_a$ for three values of the parameter d defined by $\gamma_{ba} = (1 + d)(\gamma_b + \gamma_a)/2$. In the case of iodine molecules, for which $\gamma_b/\gamma_a \geqslant 1$ for all pressures, the difference between γ_{p-p} and $\gamma_{a'a}$ is smaller than $0.05\gamma_{a'a}$ even for a very strong dephasing in the collisions. This analysis shows that our experimental study of the linewidth versus pressure yields the quantity $d\gamma_{a'a}/dP_{I_2}$ to a good approximation.

One can use expression (3.5) to discuss transit-time effects in SRR spectroscopy in comparison with usual saturation spectroscopy (with counterpropagating waves), since the saturation terms have the same structure for copropagating waves as for counterpropagating ones. It is clear that the relative influence of the terms involving, respectively, the coefficients A, B, and C depends critically on the relaxation rates $\gamma_{a'a}$ and γ_{ba} through the range of possible values for the times τ and τ'. In usual saturation spectroscopy, far from the beam waist, the coefficients C and B play the major role since A decreases as $1/z^2$ and further multiplies the time τ', which is not associated with the detuning. In SRR spectroscopy, when $\gamma_{ba}, \gamma_b \gg \gamma_a, \gamma_{a'}, \gamma_{aa'}$, first, the contribution of the saturation process (two single photon steps) is sufficiently small to be neglected; second, in the Raman term, it is now the coefficient A that plays the major role (the roles of the times τ and τ' are interchanged with respect to the previous case); hence there is a reduced transit-time broadening since A is determined by the local beam radius $w(z)$, and there is a reduced asymmetry since the range of possible values for τ is limited by γ_{ba} in the $2Bu^2\tau\tau'$ term.

As it was mentioned already, this is precisely the case of I_2 at low pressure. Figure 8 shows the result of the line-shape calculations for SRR resonances with matched divergent beams close to our experimental conditions (see Fig. 6) compared with the case of nondivergent beams. Calculated line shapes show an asymmetry but very little associated broadening. The result of the calculation with $\gamma_{aa'}/2\pi \cong 15$ kHz shows good agreement with the experiment (solid curves in Fig. 6).

If in addition to a low-pressure condition ($\gamma_{ba} \gg \gamma_{a'a}$) the divergence of the matched beams is small, we may simplify the Raman term in Eq. (3.5) to

$$I_R(\Delta) = [1/(2\gamma_{ba})]\mathrm{Re}\int_0^{+\infty} d\tau' \frac{\exp[(i\Delta - \gamma_{a'a})\tau']}{1 + \tau'^2/\tau_{tr}^2}$$
$$= (\tau_{tr}/4\gamma_{ba})\mathrm{Im}\{E_1[-(i\gamma_{a'a} + \Delta)\tau_{tr}] \times \exp[-(i\gamma_{a'a} + \Delta)\tau_{tr}] - E_1[(i\gamma_{a'a} + \Delta)\tau_{tr}] \times \exp[(i\gamma_{a'a} + \Delta)\tau_{tr}]\}, \quad (3.10)$$

which is the same line shape as in Doppler-free two-photon spectroscopy.[8]

Figure 9 shows the result of the line-shape calculations for $\tau_{tr} \simeq 18$ μs ($w_0 = 0.25$ cm and $u = 140$ m/s) and $\gamma_{a'a}/2\pi$ equal to 0.1, 1, 3, and 10 kHz. For small values of the parameter $\eta = \gamma_{a'a}\tau_{tr}$, the line shape differs from a Lorentzian and exhibits a sharp top. The second derivative of Eq. (3.10) is easily calculated to be

$$d^2I_R(\Delta)/d\Delta^2 = -[\tau_{tr}^3/(2\gamma_{ba})]\mathrm{Re}(1/[(\gamma_{a'a} - i\Delta)\tau_{tr}] + i/2\{E_1[-(i\gamma_{a'a} + \Delta)\tau_{tr}] \times \exp[-(i\gamma_{a'a} + \Delta)\tau_{tr}] - E_1[(i\gamma_{a'a} + \Delta)\tau_{tr}]\exp[(i\gamma_{a'a} + \Delta)\tau_{tr}]\}), \quad (3.11)$$

from which one can show that the peak-to-peak width of the first derivative is given by $2[(2/\pi)(\gamma_{a'a}/\tau_{tr})]^{1/2}$ in the

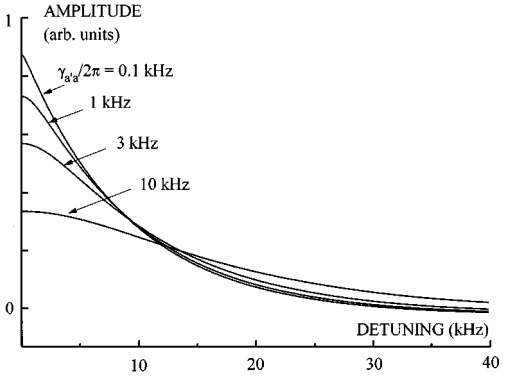

Fig. 9. Results of the line-shape calculations with $w_0 = 0.25$ cm and $\gamma_{ba}/2\pi = 100$ kHz for $\gamma_{a'a}/2\pi$ equal to 0.1, 1, 3, and 10 kHz. The sharp top of the line shape is the signature of the influence of the slow molecules.

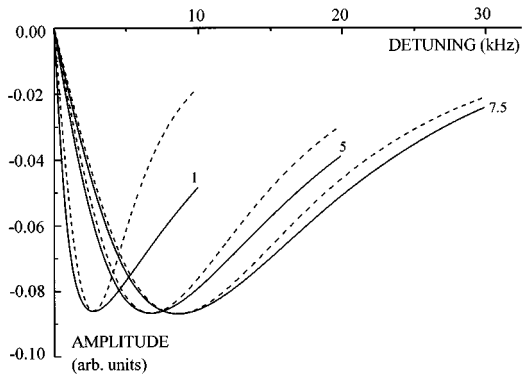

Fig. 10. First derivatives of calculated line shapes with $w_0 = 0.25$ cm and $\gamma_{ba}/2\pi = 100$ kHz for $\gamma_{a'a}/2\pi$ equal to 1, 5, and 7.5 kHz compared with first derivatives of pure Lorentzians (dashed curves). The difference between the line shape with $\gamma_{a'a}/2\pi$ equal to 7.5 kHz and the pure Lorentzian derivative (half-width equal to 13.8 kHz) could not be observed in our experiment.

transit regime. The second derivative becomes much narrower than the line shape itself as η is reduced below unity.

As in the case of saturated absorption, this phenomenon may be explained by a velocity-selection effect.[9,10] In the pure transit limit ($\eta \ll 1$) the line shape becomes a double exponential:

$$I_R(\Delta) = \pi/4(\tau_{\mathrm{tr}}/\gamma_{ba})\exp(-|\Delta|\tau_{\mathrm{tr}}), \quad \Delta \gg \gamma_{a'a}, \tag{3.12}$$

with a singular second derivative.

The conditions for this selection of slow molecules are the same as for saturation spectroscopy and are discussed in detail in Ref. 15: Besides $\eta \ll 1$, one needs to satisfy also the condition of low saturation in the experiment, $\Omega_R \tau_{\mathrm{tr}} \ll 1$, where $\Omega_R \cong \Omega_{ba}\Omega_{ba'}/\gamma_{ba}$ is the effective Rabi frequency for the Raman transition and where $\Omega_{ba,ba'}$ are the Rabi angular frequencies of the optical transitions. Expressions for these Rabi frequencies averaged over Zeeman sublevels are derived in Appendix A.

Let us give a numerical estimate for the Raman transition $(\varepsilon = 5, F = 10) \rightarrow (\varepsilon = 5, F = 9)$ and for a power of the laser beams equal to ~1 mW with a 1-cm beam radius: $\langle \Omega_{ab}^2 \rangle^{1/2} = 57389\ \mathrm{s}^{-1}$, $\langle \Omega_{a'b}^2 \rangle^{1/2} = 14774\ \mathrm{s}^{-1}$, and $\gamma_{ba} = 2\pi \times 10^5\ \mathrm{s}^{-1}$ give $\Omega_R = 1349\ \mathrm{s}^{-1}$ and $\Omega_R \tau_{\mathrm{tr}} \simeq 0.1$.

In the case of a uniform illumination with an intensity of 1 mW/cm^2 over a 0.25-cm-radius diaphragm, the effective Rabi frequency for the Raman transition is only $\pi/2$ higher, while τ_{tr} is of the order of 3 or 4 times smaller; hence there is an even smaller saturation parameter $\Omega_R \tau_{\mathrm{tr}}$. Therefore the laser power used for the experiment of Fig. 5 (curve b) was in a good range for the observation of line-shape distortions due to slow molecules.

The reason why no significant departure of the line shape from a pure Lorentzian was observed in our experiments could have two origins *a priori*:

(1) a slight misalignment of the two beams in the cell;

(2) a higher relaxation rate than expected, possibly owing to some foreign gas residual pressure, leading to a too large value of the parameter η.

A small angle θ between the laser beams at frequencies ν_1 and ν_2 leads to the residual Doppler broadening $k_x u \sim k\theta u$ described by formula (3.8). We estimate that θ should not exceed a few times 10^{-5} rad, in which case the Doppler broadening can at most be comparable to the transit-time broadening. Furthermore, if the contribution of slow molecules is dominant, this residual effect should also decrease.

Figure 10 shows calculated line shapes for the first derivative of Raman resonances under conditions close to the experimental ones with $\gamma_{a'a}/2\pi$ equal to 1, 5, or 7.5 kHz. When compared with the first derivative of a pure Lorentzian (dashed curves), the calculated line shape for $\gamma_{a'a}/2\pi$ equal to 7.5 kHz shows only a small difference that is difficult to observe with a limited experimental signal-to-noise ratio. The half-width (HWHM) of the calculated line shape for $\gamma_{p-p}/2\pi = 13.8$ kHz is in good agreement with the experimentally measured value, which is 14 kHz.

This analysis is therefore consistent with a value of $\eta \sim 1$, which can only be understood as coming from a residual foreign gas pressure that is still not well enough controlled in the present stage of the experiment.

4. SUMMARY

As a conclusion, the experimental method presented here gives the possibility of accurate and independent measurements of the lower-level hyperfine structure of molecules. As it was shown in Refs. 3 and 13, independent measurements of the hyperfine interaction constants of the lower level together with the measurement of the hyperfine structure of the $X \rightarrow B$ transitions improve the accuracy of the fitting procedure that is used to evaluate the constants of hyperfine interactions.

The results of the line-shape calculations explain the main features of the SRR resonances. As far as only the divergence of the laser beam is concerned, the behavior of the SRR resonances differs strongly from the case of saturated absorption. The SRR resonances probe the local size of the laser beam and are relatively insensitive to the beam divergence or to wave-front distortions by cell windows. In the transit-time broadening limit, i.e., when $u/w \gg \gamma_{a'a}$, and without beam curvature, the theory predicts for the SRR resonance a double exponential line shape with a sharp top. As in the case of saturated absorption, this phenomenon may be explained by a velocity-selection effect.[9,10] This regime could not quite be reached in the present experiments, but we have analyzed the difficulties that should be overcome to reach it:

(1) The filling of the iodine cells appears to be critical, since the residual foreign gas is presently the main limitation, and requires further efforts.

(2) The parallelism between the beams at frequencies ν_1 and ν_2 in the cell should be better than 10^{-5} rad, and this point may require some more care in future experiments, although we expect that the enhanced relative contribution of slow molecules should also reduce the residual Doppler broadening.

Our estimate of the signal-to-noise ratio shows that, when these difficulties are solved and with a beam diam-

eter of the order of 1–2 cm in a low-pressure cell, one should be able to reach the kilohertz linewidth for SRR resonances (and possibly beyond with a much longer effective path in iodine), thus opening useful new perspectives for high-precision spectroscopy and for metrology.

APPENDIX A: EVALUATION OF THE DENSITY-MATRIX DIAGRAMS CORRESPONDING TO THE STIMULATED RAMAN PROCESS AND TO THE SATURATED ABSORPTION PROCESS

The three diagrams corresponding to the stimulated Raman process, the saturation term, and the dynamical Stark effect are given in Figs. 11, 12, and 13 with the associated diagrammatic rules and the same notations as in Ref. 7.

The two beams propagate along the z axis with wave vectors $\mathbf{k}_1$ and $\mathbf{k}_2$. Both beams are assumed to be Gaussian (TEM_{00} mode). In this case the complex representation of the electric field is given by

$$\mathbf{E} = \mathbf{E}_0 U(\mathbf{r}) \exp[i(\omega t - kz + \varphi)] \tag{A1}$$

with

$$U(\mathbf{r}) = L(z) \exp\left[-L(z)\,\frac{x^2 + y^2}{w_0^2}\right]. \tag{A2}$$

The function

$$L(z) = \frac{1}{1 - 2i(z - z_0)/b} \tag{A3}$$

is a complex Lorentzian with a total width equal to the confocal parameter $b = kw_0^2$ (w_0 is the radius of the beam waist located at z_0). Then, for any position z, the waist $w(z)$ and the wave-front radius of curvature $R(z)$ are given by

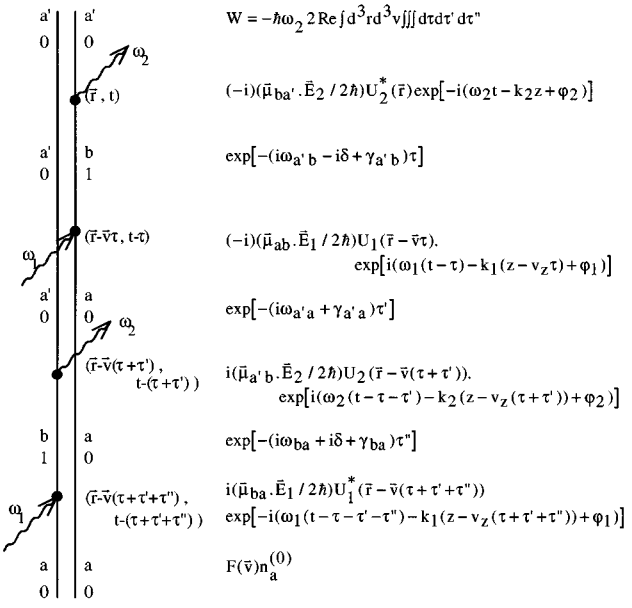

Fig. 11. Double time-ordered Feynman diagram for the Raman process.

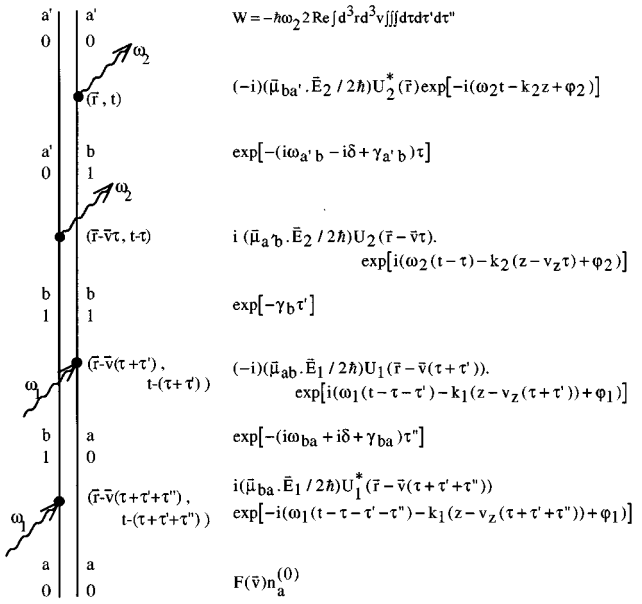

Fig. 12. Double time-ordered Feynman diagram for the saturation process.

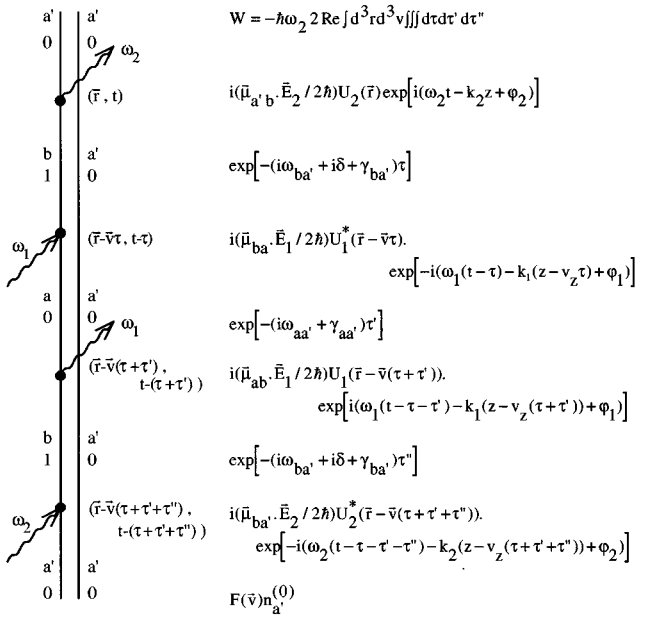

Fig. 13. Double time-ordered Feynman diagram for the dynamical Stark effect.

$$L(z) = \frac{w_0^2}{w^2(z)} + i\,\frac{b}{2R(z)}. \tag{A4}$$

In what follows, the parameters of the two beams are labeled by 1 and 2, respectively. The gas in the cell is in thermodynamic equilibrium, and the velocity distribution is the usual Maxwell–Boltzmann distribution:

$$F_1(v_z) = (1/\sqrt{\pi}u)\exp(-v_z^2/u^2), \tag{A5}$$

$$F_2(v_\perp) = (2v_\perp/u^2)\exp(-v_\perp^2/u^2), \tag{A6}$$

where $u = (2k_BT/M)^{1/2}$ is the most probable velocity.

Concerning the stimulated Raman process (Fig. 11), the power absorbed per unit length for the laser beam 2 (ω_2) is found to be

$$\begin{aligned} dW/dz = & -2n_a^{(0)}\Pi_\Omega \hbar\omega_2 \int d^3v F(\mathbf{v}) \int_{-\infty}^{+\infty} dx \\ & \times \int_{-\infty}^{+\infty} dy \ \mathrm{Re} \int_0^{+\infty} d\tau \int_0^{+\infty} d\tau' \int_0^{+\infty} d\tau'' \\ & \times U_2^*(\mathbf{r}) U_1(\mathbf{r} - \mathbf{v}\tau) U_2[\mathbf{r} - \mathbf{v}(\tau + \tau')] \\ & \times U_1^*[\mathbf{r} - \mathbf{v}(\tau + \tau' + \tau'')] \exp[ik_2 v_z(\tau + \tau') \\ & - ik_1 v_z(\tau' + \tau'')] \exp[-i\omega_2\tau + i(\omega_1 - \omega_2)\tau' \\ & + i\omega_1\tau''] \exp[-(i\omega_{a'b} + \gamma_{a'b})\tau - (i\omega_{a'a} \\ & + \gamma_{a'a})\tau' - (i\omega_{ba} + \gamma_{ba})\tau''], \end{aligned} \tag{A7}$$

where $\Pi_\Omega = (\boldsymbol{\mu}_{ba'} \cdot \mathbf{E}_2/2\hbar)(\boldsymbol{\mu}_{ab} \cdot \mathbf{E}_1/2\hbar)(\boldsymbol{\mu}_{a'b} \cdot \mathbf{E}_2/2\hbar) \times (\boldsymbol{\mu}_{ba} \cdot \mathbf{E}_1/2\hbar)$. The integration on v_z is performed in the infinite-Doppler-width limit, and we obtain

$$\begin{aligned} dW/dz = & -n_a^{(0)}\hbar\omega_2(4\sqrt{\pi}/ku)\Pi_\Omega \int_{-\infty}^{+\infty} dv_x F_1(v_x) \\ & \times \int_{-\infty}^{+\infty} dv_y F_1(v_y) \int_{-\infty}^{+\infty} dx \int_{-\infty}^{+\infty} dy \\ & \times \mathrm{Re} \int_0^{+\infty} d\tau \int_0^{+\infty} d\tau' U_2^*(\mathbf{r}) U_1(\mathbf{r} - \mathbf{v}_\perp\tau) \\ & \times U_2[\mathbf{r} - \mathbf{v}_\perp(\tau + \tau')] U_1^*[\mathbf{r} - \mathbf{v}_\perp(2\tau + \tau')] \\ & \times \exp[(i\Delta - 2\gamma_{ba})\tau] \exp[(i\Delta - \gamma_{a'a})\tau'], \end{aligned} \tag{A8}$$

where $(\omega_1 - \omega_2)\omega_{ba'}/\omega_2 - \omega_{a'a}$ is approximated by the frequency detuning $\Delta = (\omega_1 - \omega_2) - \omega_{a'a}$. In this expression the longitudinal transit-time effect is neglected, and $\mathbf{v}$ is replaced by $\mathbf{v}_\perp$ in the functions U_1 and U_2. The cylindrical symmetry of Gaussian beams allows us to choose coordinates such that $v_x = v_\perp$ and $v_y = 0$. We find

$$\begin{aligned} dW/dz = & -n_a^{(0)}\Pi_\Omega \hbar\omega_2(4\sqrt{\pi}/ku)\Lambda(z) \int_0^{+\infty} dv_\perp F_2(v_\perp) \\ & \times \int_{-\infty}^{+\infty} dx \int_{-\infty}^{+\infty} dy \mathrm{Re} \int_0^{+\infty} d\tau \int_0^{+\infty} d\tau' \\ & \times \exp[-l_2^*(x^2 + y^2)] \exp\{-l_1[(x - v_\perp\tau)^2 \\ & + y^2]\} \exp(-l_2\{[x - v_\perp(\tau + \tau')]^2 + y^2\}) \\ & \times \exp(-l_1^*\{[x - v_\perp(2\tau + \tau')]^2 + y^2\}) \\ & \times \exp[(i\Delta - 2\gamma_{ba})\tau] \exp[(i\Delta - \gamma_{a'a})\tau'], \end{aligned} \tag{A9}$$

with $\Lambda(z) = L_1(z)L_1^*(z)L_2(z)L_2^*(z)$, $l_1 = L_1(z)/w_{01}^2$, and $l_2 = L_2(z)/w_{02}^2$. The integrations on x and y give the expression

$$\begin{aligned} dW/dz = & -n_a^{(0)}\Pi_\Omega \hbar\omega_2(2\sqrt{\pi}/ku)S(z) \int_0^{+\infty} dv_\perp F_2(v_\perp) \\ & \times \mathrm{Re} \int_0^{+\infty} d\tau \int_0^{+\infty} d\tau' \\ & \times \exp[-v_\perp^2(A_R\tau'^2 + 2B_R\tau\tau' + C_R\tau^2)] \\ & \times \exp[(i\Delta - 2\gamma_{ba})\tau] \exp[(i\Delta - \gamma_{a'a})\tau'], \end{aligned} \tag{A10}$$

where $S(z) = \pi\Lambda(z)/[1/w_1^2(z) + 1/w_2^2(z)]$. The coefficients A_R, B_R, and C_R depend only upon the beam geometry:

$$A_R = \frac{(l_1 + l_2^*)(l_1^* + l_2)}{l_1 + l_2^* + l_1^* + l_2}, \tag{A11}$$

$$B_R = \frac{l_1^*(l_1 + l_2^*) + l_2^*(l_1^* + l_2)}{l_1 + l_2^* + l_1^* + l_2}, \tag{A12}$$

$$C_R = \frac{(l_1 + l_2)(l_1^* + l_2^*) + 4l_1^*l_2^*}{l_1 + l_2^* + l_1^* + l_2}. \tag{A13}$$

We also use the quantity D_R:

$$D_R = C_R - B_R^2/A_R. \tag{A14}$$

The integration over τ' would give the line shape for each transverse velocity class $v_\perp$ as a Fourier transform over τ as in Ref. 9. This form is interesting to display the inhomogeneous character of the line shape, with the narrowest contributions coming from the slow molecules.

On the other hand, the integration on $v_\perp$ gives

$$\begin{aligned} dW/dz = & -n_a^{(0)}\Pi_\Omega \hbar\omega_2(2\sqrt{\pi}/ku)S(z)\mathrm{Re} \int_0^{+\infty} d\tau \\ & \times \int_0^{+\infty} d\tau' \exp[(i\Delta - 2\gamma_{ba})\tau] \\ & \times \exp[(i\Delta - \gamma_{a'a})\tau']/(1 + A_R u^2\tau'^2 \\ & + 2B_R u^2\tau\tau' + C_R u^2\tau^2). \end{aligned} \tag{A15}$$

The integration on τ' gives

$$\begin{aligned} dW/dz = & -n_a^{(0)}\Pi_\Omega \hbar\omega_2(2\sqrt{\pi}/ku)S(z)\mathrm{Im}(\gamma_{a'a} \\ & - i\Delta)/(2A_R u^2) \int_0^{+\infty} d\tau \exp[(i\Delta - 2\gamma_{ba})\tau] \\ & \times [\exp(Z_{R2})E_1(Z_{R2}) \\ & - \exp(Z_{R1})E_1(Z_{R1})]/Y_R, \end{aligned} \tag{A16}$$

where E_1 is the exponential integral function and

$$Z_{R1} = X_R + iY_R,$$

$$Z_{R2} = X_R - iY_R,$$

$$X_R = \tau(\gamma_{a'a} - i\Delta)B_R/A_R,$$

$$Y_R = (\gamma_{a'a} - i\Delta)[1/(u\sqrt{A_R})]\sqrt{1 + D_R u^2\tau^2}.$$

The diagram corresponding to the saturated absorption process with copropagating beams is given in Fig. 12, and the power absorbed per unit length for laser beam 2 at ω_2 is

$$\begin{aligned} dW/dz = & -2n_a^{(0)}\Pi_\Omega \hbar\omega_2 \int d^3v F(\mathbf{v}) \int_{-\infty}^{+\infty} dx \int_{-\infty}^{+\infty} dy \\ & \times \mathrm{Re} \int_0^{+\infty} d\tau \int_0^{+\infty} d\tau' \int_0^{+\infty} d\tau'' U_2^*(\mathbf{r}) U_2(\mathbf{r} \\ & - \mathbf{v}\tau) U_1[\mathbf{r} - \mathbf{v}(\tau + \tau')] U_1^*[\mathbf{r} - \mathbf{v}(\tau + \tau' \\ & + \tau'')] \exp(ik_2 v_z \tau - ik_1 v_z \tau'') \exp(-i\omega_2 \tau \\ & + i\omega_1 \tau'') \exp[-(i\omega_{a'b} - i\delta + \gamma_{a'b})\tau - \gamma_b \tau' \\ & - (i\omega_{ba} + i\delta + \gamma_{ba})\tau''] . \end{aligned} \tag{A17}$$

Following the same calculation as in the case of the stimulated Raman process, an expression similar to Eq. (A15) is obtained:

$$\begin{aligned} dW/dz = & -n_a^{(0)}\Pi_\Omega \hbar\omega_2 (2\sqrt{\pi}/ku) S(z) \mathrm{Re} \int_0^{+\infty} d\tau \\ & \times \int_0^{+\infty} d\tau' \exp[(i\Delta - 2\gamma_{ba})\tau] \\ & \times \exp(-\gamma_b \tau')/(1 + A_S u^2 \tau'^2 \\ & + 2B_s u^2 \tau\tau' + C_S u^2 \tau^2) . \end{aligned} \tag{A18}$$

The geometrical coefficients A_S, B_S, and C_S are given by

$$A_S = \frac{(l_1 + l_1^*)(l_2^* + l_2)}{l_1 + l_2^* + l_1^* + l_2}, \tag{A19}$$

$$B_S = \frac{l_1^*(l_2 + l_2^*) + l_2^*(l_1^* + l_1)}{l_1 + l_2^* + l_1^* + l_2}, \tag{A20}$$

$$C_S = \frac{(l_1 + l_2)(l_1^* + l_2^*) + 4l_1^* l_2^*}{l_1 + l_2^* + l_1^* + l_2}, \tag{A21}$$

and D_S is defined by

$$D_S = C_S - B_S^2/A_S . \tag{A22}$$

Finally, the integration on τ' gives

$$\begin{aligned} dW/dz = & -n_a^{(0)}\Pi_\Omega \hbar\omega_2 (\sqrt{\pi}/ku) S(z) \gamma_b/(A_S u^2) \\ & \times \mathrm{Im} \int_0^{+\infty} d\tau \exp[(i\Delta - 2\gamma_{ba})\tau] \\ & \times [\exp(Z_{S2}) E_1(Z_{S2}) \\ & - \exp(Z_{S1}) E_1(Z_{S1})]/Y_S , \end{aligned} \tag{A23}$$

with

$$Z_{S1} = X_S + iY_S , \quad Z_{S2} = X_S - iY_S ,$$

$$X_S = \gamma_b \tau B_S/A_S , \quad Y_S = \gamma_b/(u\sqrt{A_S})\sqrt{1 + D_S u^2 \tau^2} .$$

The contribution of the dynamical Stark effect given by Fig. 13 is negligible in the present experiment for which $k_1 \simeq k_2$.

In the case of degenerate levels the products of four Rabi frequencies,

$$\begin{aligned} \Pi_\Omega = & \sum_{M_b' M_{a'} M_b M_a} \langle bF_b M_b' | \boldsymbol{\mu} \cdot \mathbf{E}_2^* | a'F_{a'} M_{a'} \rangle \langle aF_a M_a | \boldsymbol{\mu} \\ & \cdot \mathbf{E}_1 | bF_b M_b' \rangle \langle a'F_{a'} M_{a'} | \boldsymbol{\mu} \cdot \mathbf{E}_2 | bF_b M_b \rangle \langle bF_b M_b | \boldsymbol{\mu} \\ & \cdot \mathbf{E}_1^* | aF_a M_a \rangle / (16\hbar^4) , \end{aligned} \tag{A24}$$

can be calculated as in Appendix B of Ref. 7 by use of an irreducible tensor basis in Liouville space. Assuming well-defined polarizations q_1 and q_2 for the two fields, one finds from Eq. (B-10) of Ref. 7 that

$$\begin{aligned} \Pi_\Omega = & A_{abba'} |\langle bF_b \| \mu \| aF_a \rangle|^2 |\langle bF_b \| \mu \| a'F_{a'} \rangle|^2 \\ & \times E_1^2 E_2^2 / (16\hbar^4) , \end{aligned} \tag{A25}$$

where the angular factors $A_{abba'}$ are given by

$$\begin{aligned} A_{abba'} = & \sum_{K,Q} (2K + 1) \\ & \times \begin{pmatrix} K & 1 & 1 \\ Q & -q_1 & q_2 \end{pmatrix}^2 \begin{Bmatrix} K & 1 & 1 \\ F_b & F_a & F_{a'} \end{Bmatrix}^2 \end{aligned} \tag{A26}$$

in the case of the Raman diagram and

$$\begin{aligned} A_{abba'} = & (-1)^{q_1 + q_2 + F_a + F_{a'}} \sum_{K=0,1,2} (2K + 1) \\ & \times \begin{pmatrix} K & 1 & 1 \\ 0 & -q_1 & q_1 \end{pmatrix} \begin{pmatrix} K & 1 & 1 \\ 0 & -q_2 & q_2 \end{pmatrix} \\ & \times \begin{Bmatrix} K & 1 & 1 \\ F_{a'} & F_b & F_b \end{Bmatrix} \begin{Bmatrix} K & 1 & 1 \\ F_a & F_b & F_b \end{Bmatrix} \end{aligned} \tag{A27}$$

in the case of the saturation diagram.

As expected from expression (A25), these two formulas are equivalent and give results identical to those obtained for saturation spectroscopy in the case of crossover resonances with a common upper level. The coefficients $A_{abba'}$ are tabulated in Table 1 of Ref. 12 for the present experiments with $q_1 = 0$ and $q_2 = 1$, the beam polarizations being, respectively, π and σ. For example, with $F_b = 9$, $F_a = 10$, and $F_{a'} = 9$: $A_{abba'} = 0.006842$.

The reduced matrix elements of the electric dipole operator are also given in Ref. 12 as

$$|\langle Xv''J''\varepsilon''F'' \| \mu \| Bv'J'\varepsilon'F' \rangle|^2 = \mu_e^2 |\langle v' | v'' \rangle|^2 S_{J''J'} \Phi_{F''F'} \tag{A28}$$

with

$$\begin{aligned} \Phi_{F'F''} = & (2F' + 1)(2F'' + 1) \\ & \times \left| \sum_I \alpha''^*(I, \varepsilon'', J'', F'') \alpha'(I, \varepsilon', J', F') \right. \\ & \times \left. \begin{Bmatrix} J'' & 1 & J' \\ F' & I & F'' \end{Bmatrix} \right|^2 . \end{aligned} \tag{A29}$$

These various quantities are also given in Ref. 12:

- The electronic transition moment $\mu_e^2 = 0.95$ (Debye)^2.

• The Franck–Condon factor $|\langle v'|v''\rangle|^2 = 1.779 \times 10^{-2}$ for $v' = 43$, $v'' = 0$; and $J' = J'' = 14$.

• The rotational line strength $S_{J''J'}$ equal to J'' for the P branch and J' for the R branch.

• The hyperfine factors $\Phi_{F'F''}$ have to be calculated for each hyperfine transition. As examples, $\Phi_{F'F''} = 0.7122$ for the a_7 line ($F' = 9$, $F'' = 10$) and $\Phi_{F'F''} = 0.0472$ for the connected ($F' = 9$, $F'' = 9$)line.

We are now in a position to calculate numerically the expected signals. An interesting intermediate calculation is that of the linear absorption coefficient at the center of the Doppler profile:

$$k_{ab} = n_{M_a}^{(0)} \frac{1}{4\pi\varepsilon_0} \frac{8\pi^3\nu}{3hc} \frac{2\sqrt{\pi}}{ku} |\langle bF_b\|\mu\|aF_a\rangle|^2, \tag{A30}$$

where $n_{M_a}^{(0)} = n_a^{(0)}/g_a$ is the population of a Zeeman sublevel of the lower level a.

This population is given by

$$n_{M_a}^{(0)} = (N/Z)\exp[-E_a/(k_BT)],$$

where $N = 3.2958 \times 10^{22}$ molecules/m^3 for 1 Torr at 293 K and where Z is the partition function:

$$Z = Z_{\text{vib}} Z_{\text{rot,nucl}}.$$

The vibrational partition function is (with zero energy for the ground vibrational state)

$$Z_{\text{vib}} = \frac{1}{1 - \exp(-\Theta_{\text{vib}}/T)} \tag{A31}$$

with $\Theta_{\text{vib}} = h\nu_{\text{vib}}/k_B = 308.664$ K so that $Z_{\text{vib}}(293\text{ K}) = 1.535$.

The rotational partition, taking into account the Fermionic character of the iodine nucleus of spin $i = 5/2$, is

$$\begin{aligned} Z_{\text{rot,nucl}} &= i(2i+1) \sum_{J\ \text{even}} (2J+1) \\ &\quad \times \exp[-J(J+1)\Theta_r/T] + (i+1)(2i+1) \\ &\quad \times \sum_{J\ \text{odd}} (2J+1)\exp[-J(J+1)\Theta_r/T] \\ &\simeq (2i+1)^2 \frac{T}{2\Theta_r} \end{aligned} \tag{A32}$$

with $\Theta_r = hcB_0/k_B = 0.05368$ K so that $Z_{\text{rot,nucl}}(293\text{ K}) = 98249$.

As an example, for the $v'' = 0$, $J'' = 13$ levels, the population $n_{M_a}^{(0)}$ in each Zeeman sublevel of each hyperfine level is 2.114×10^{17} molecules/m^3 for 1 Torr at 293 K.

From Eqs. (A28)–(A32) we find that

$$k_{ab} = n_a^{(0)} 4\pi^{3/2} \frac{c}{u} \alpha \frac{|\langle bF_b\|\mu\|aF_a\rangle|^2}{3g_a e^2}, \tag{A33}$$

where $\alpha = e^2/4\pi\varepsilon_0\hbar c$ is the fine structure constant, is equal to 1.68 m^{-1} Torr^{-1} for the a_7 line at 293 K.

The quantity $\alpha|\langle bF_b\|\mu\|aF_a\rangle|^2/3g_a e^2$, which is equal to $1.077 \times 10^{-24}\alpha$ m^2 in this case, plays the role of a cross section averaged over Zeeman sublevels.

For the associated weak transition ($F' = 9$, $F'' = 9$) the absorption coefficient is smaller by the ratio of the Φ coefficients 0.7122/0.0472 = 15.09, which gives $k_{a'b} = 0.111$ m^{-1} Torr^{-1}.

The absorption coefficient corresponding to the nonlinear processes (Raman or saturation terms) is now expressed with the linear absorption coefficient. From expressions (A15) and (A18) (in which one should also divide the population $n_a^{(0)}$ by the degeneracy factor g_a) we have

$$\begin{aligned} k_{R,S} &= -(2\sqrt{\pi}/ku) \frac{n_a^{(0)}}{g_a} \hbar\omega_2 S(z)\mu_e^4 |\langle v'|v''\rangle|^4 \\ &\quad \times S_{J''J'}^2 \Phi_{ab}\Phi_{a'b} A_{abba'} [E_1^2 E_2^2/(16\hbar^4)] I_{R,S}(\Delta) \\ &\quad \times \left[c\varepsilon_0 E_2^2/2 \int U_2 U_2^* \mathrm{d}x\mathrm{d}y\right]^{-1}. \end{aligned} \tag{A34}$$

At the beam waist,

$$\begin{aligned} k_{R,S} &= -\left[\frac{\sqrt{\pi}}{ku} \frac{n_a^{(0)}}{g_a} \omega_2 \frac{\mu_e^2 |\langle v'|v''\rangle|^2 S_{J''J'}\Phi_{a'b}}{3\varepsilon_0\hbar c}\right] \\ &\quad \times 3A_{abba'} \frac{\mu_e^2 |\langle v'|v''\rangle|^2 S_{J''J'}\Phi_{ab}E_1^2}{4\hbar^2} I_{R,S}(\Delta) \\ &= -k_{a'b}(9g_b A_{abba'})\langle\Omega_{ab}^2\rangle I_{R,S}(\Delta), \end{aligned} \tag{A35}$$

where $(9g_b A_{abba'})$ is an angular factor close to one and where

$$\langle\Omega_{ab}^2\rangle = \frac{\mu_e^2 |\langle v'|v''\rangle|^2 S_{J''J'}\Phi_{ab}}{3g_b} \frac{E_1^2}{4\hbar^2} \tag{A36}$$

is a Rabi frequency squared averaged over Zeeman sublevels.

As an example of interest to our experiment, let us calculate this quantity for the a_7 line. Using a laser power $P_1 = (\pi/4)c\varepsilon_0 E_1^2 w_1^2$ equal to 1 mW, we find $\langle\Omega_{ab}^2\rangle^{1/2} = 57389$ s^{-1}.

For the Raman signal in the collisional regime we have $I_R(0) = 1/(2\gamma_{ba}\gamma_{a'a})$. Taking $\gamma_{ba} = 2\pi \times 10^5$ s^{-1} and $\gamma_{a'a} = 2\pi \times 8 \times 10^3$ s^{-1}, corresponding to the 0.2 mTorr pressure, we find a saturation parameter $\langle\Omega_{ab}^2\rangle/(2\gamma_{ba}\gamma_{a'a}) = 5.2 \times 10^{-2}$. For the $L = 50$ cm cell, formula (A35) gives an absorption $|k_R L| = 0.68 \times 10^{-6}$, in good agreement with the order of magnitude of the experimental measurement reported in the text.

*Also with Laboratoire de Gravitation et Cosmologie Relativistes, Unité de Recherche Associée au Centre National de la Recherche Scientifique 769, Université Pierre et Marie Curie, Paris, France.

**Permanent address: Institute of Laser Physics, Siberian Branch of the Russian Academy of Sciences, Novosibirsk, Russia.

REFERENCES

1. I. M. Beterov and V. P. Chebotayev, in *Progress in Quantum Electronics*, J. H. Sanders and S. Stenholm, eds. (Pergamon, London, 1974), Vol. 3, Pt. 1, p. 3, and references therein; P. R. Hemmer, M. S. Shahriar, V. D. Natoli, and S. Ezekiel, J. Opt. Soc. Am. B **6**, 1519 (1989), and references therein.

2. P. R. Hemmer, S. Ezekiel, and C. C. Leiby, Jr., Opt. Lett. **8**, 440 (1983).
3. A. Yokozeki and J. S. Muenter, J. Chem. Phys. **72**, 3796 (1980).
4. Th. Hänsch and P. Toschek, Z. Phys. **236**, 213 (1970), and references therein.
5. S. A. J. Druet, J.-P. E. Taran, and Ch. J. Bordé, J. Phys. (Paris) **40**, 819 (1979).
6. S. A. J. Druet, J.-P. E. Taran, and Ch. J. Bordé, J. Phys. (Paris) **41**, 183 (1980).
7. Ch. J. Bordé, in *Advances in Laser Spectroscopy*, F. T. Arecchi, F. Strumia, and H. Walther, eds. (Plenum, New York, 1983), p. 1.
8. Ch. J. Bordé, C. R. Acad. Sci. Ser. B **282**, 341 (1976).
9. Ch. J. Bordé, J. L. Hall, C. V. Kunasz, and D. G. Hummer, Phys. Rev. A **14**, 236 (1976).
10. E. V. Baklanov, B. Y. Dubetskii, V. M. Semibalamut, and E. A. Titov, Sov. J. Quantum Electron. **5**, 1374 (1976).
11. J. E. Thomas and W. W. Quivers, Jr., Phys. Rev. A **22**, 2115 (1980).
12. Ch. J. Bordé, G. Camy, and B. Decomps, Phys. Rev. A **20**, 254 (1979).
13. Ch. J. Bordé, G. Camy, B. Decomps, J. P. Descoubes, and J. Vigué, J. Phys. (Paris) **42**, 1393 (1981).
14. A. N. Goncharov, M. N. Skvortsov, and V. P. Chebotayev, Appl. Phys. B **51**, 108 (1990).
15. Ch. Chardonnet, F. Guernet, G. Charton, and Ch. J. Bordé, Appl. Phys. B **59**, 333 (1994), and references therein.